THE SURFACE RECONSTRUCTIONS OF THE (100) CRYSTAL FACES OF IRIDIUM, PLATINUM AND GOLD

II. Structural determination by LEED intensity analysis

M.A. VAN HOVE, R.J. KOESTNER, P.C. STAIR [a], J.P. BIBÉRIAN [b],
L.L. KESMODEL [c], I. BARTOŠ [d] and G.A. SOMORJAI

Materials and Molecular Research Division, Lawrence Berkeley Laboratory and Department of Chemistry, University of California, Berkeley, California 94720, USA

The investigation, in a companion paper, of the reconstructions of the Ir(100), Pt(100), and Au(100) crystal surfaces is completed here with an extensive analysis of low energy electron diffraction (LEED) intensities, using dynamical (multiple scattering) calculations. It is found that a hexagonal rearrangement of the top monolayer is a likely explanation of the surface reconstruction. At least for Ir and Pt (no calculations were made for Au), this hexagonal layer would have a registry involving bridge sites on the next square unit cell metal layer and it is contracted and buckled. Bond length contractions parallel and perpendicular to the surface occur; the Pt top layer is rotated by a small angle (0.7°) with respect to the substrate. A second model that cannot be ruled out by the LEED analysis, but disagrees with ion-scattering data, involves shifted close-packed rows of top-layer atoms and requires domain structures in the case of Pt and Au. Charge-density-wave and missing-row models are ruled out by our structure analysis. A correlation is found between the occurrence of surface reconstructions on metals and a small ratio of their Debye temperature to their melting point. This correlation singles out mainly the 5d metals as having a propensity to surface reconstruction. The effects of adsorbates on the reconstructions are also discussed.

1. Introduction

In the preceding paper, hereafter referred to as paper I, we analyzed the experimental information contained in the two-dimensional diffraction patterns of recon-

---

[a] Present address: Department of Chemistry, Northwestern University. Evanston, Illinois 60201, USA.

[b] Permanent address: Centre des Mécanismes de la Croissance Cristalline, UER Luminy, 70 Route Léon-Lachamp, F-13288 Marseille Cedex 2, France.

[c] Present address: Department of Physics, Indiana University, Bloomington, Indiana 47405, USA.

[d] Permanent address: Institute of Solid State Physics, Czechoslovak Academy of Sciences, 16253 Prague 6, Czechoslovakia.

structed Ir(100), Pt(100), Au(100) and Au(111). That analysis, together with the measurement of LEED intensity data for Ir(100)(1 × 5) and Pt(100)($_{-1}^{14}$ $_5^1$), pre-pared the way for the detailed structural investigation of the atomic locations at these surfaces described in the present paper. It is based on the analysis of the measured LEED intensities with dynamical (multiple scattering) calculations.

As Ir(100) has the surface reconstruction with the smallest unit cell, thereby providing the simplest case for LEED calculations, we concentrate our efforts on this surface, analyzing many of the structures discussed in the preceding paper. We also make calculations with a few structural models for the Pt(100)($_{-1}^{14}$ $_5^1$) surface, using suitable approximations (with minor consequences) to deal with the very large unit cell. The results will be discussed in terms of the mechanism of recon-struction and a comparison with other surface structures will be given.

2. Dynamical LEED theory

2.1. Methods used

The large unit cells of the models to be analyzed by dynamical LEED calcula-tions present special computational problems for the existing theories. First, many beams occur, giving rise to high-dimensional interlayer diffraction matrices. Second, many atoms fit in the unit cell, giving rise to high-dimensional intralayer multiple scattering matrices. We adopt the "combined space method" [1], in which the spherical wave representation is used within each layer. The top reconstructed layer counts as one layer containing 5 or 6 atoms in the unit cell. The plane wave repre-sentation is used between these layers. The Renormalized Forward Scattering (RFS) method [2] is used for the interlayer wave propagation. The intralayer mul-tiple scattering is treated by the Matrix Inversion method [1,2] for the strongly scattering platinum and by the Reverse Scattering Perturbation (RSP) method [1] for the less strongly scattering iridium. That iridium behaves relatively kinemati-cally in LEED has been noticed before [3], but we have no explanation for it. Both RSP and RFS are allowed to converge to essentially the exact result and therefore involve no neglect of important scattering events.

2.2. Physical parameters

The iridium atomic potential employed here, due to Arbman and Hoernfelt [4], has been used before in studies of Ir(111) [3] and Ir(110) [5] (the latter either reconstructed or overlayer-covered). The agreement between theory and experi-ment was often not as good as with many other metals, and this difficulty is thought to stem partly from the use of an inadequate potential: therefore we expect a corresponding measure of disagreement in the present case. A modification of this potential by Feder [6] to include relativistic spin effects has also been

applied in this work, but does not produce a noticeable improvement (as was already the case for Ir(110)(1 × 2)). The platinum potential [7] has also been used previously, namely in studies of Pt(111) [8] and unreconstructed Pt(100) [9]. This potential appears to be better than the iridium potential, but is again not as good as the potential used for a number of other metals. In this work, a relativistic spin correction to the potential is tried as well [6], with the same inconclusive result as for iridium (the same result was also found in a study of Pt(111) [8b]).

The number of phase shifts used in our calculations is mostly 6 (l_{max} = 5) for an energy range up to 120 eV for iridium and 100 eV for platinum. (Some platinum calculations were made with 5 phase shifts, but for platinum 5 phase shifts are not sufficient at the higher energies). The real part V_{or} of the inner potential (muffin-tin constant) is set to 15 eV for iridium and 14.3 eV for platinum, based on results of previous work, and is fitted a posteriori to experiment by shifting the zero point of energy. The imaginary part of the potential is set to a constant 5 eV for iridium and 4 eV for platinum and Debye temperatures of 236 and 193 K, respectively, are used for all layers (these are reduced from bulk values to allow for enhanced atomic vibrations of the surface).

2.3. Geometrical aspects

Many of the (1 × 5) models discussed and illustrated in section 5 of paper I have structures with a pair of orthogonal mirror planes, e.g. the hexagonal models with two-bridge registry and with top/center registry (cf. fig. 9 of paper I), the missing row hexagonal model, the shifted-row models (cf. fig. 11 of paper I) and the charge-density-wave model with an appropriate phase of the deformation wave. This symmetry is then exploited at normal incidence in our calculations to considerably reduce the computational effort [1]. For the same reason, off-normal incidence calculations are performed only for incidence directions retaining one mirror plane.

Among the large-unit-cell models, we chose to test the hexagonal model for the Pt(100)($_{-1}^{14}$ $_5^1$) structure since it is based on the most popular suggestion for the reconstruction. For this purpose it is necessary to make some simplifications since the top layer contains about 88 atoms in the unit cell and the number of beams is 71 times as large as with the unreconstructed surface. As one sees in fig. 6 of paper I, the ($_{-1}^{14}$ $_5^1$) unit cell can be regarded as being composed of 14 successive (1 × 5) units. The diffraction by the entire ($_{-1}^{14}$ $_5^1$) unit cell is then simply the sum of the interfering diffraction amplitudes from each of those 14 (1 × 5) units. In the case of the abrupt dislocation model of the hexagonal top layer (cf. fig. 10 of paper I) most of the 14 (1 × 5) units are identical with only a few different ones near the dislocations. This arrangement can then be simulated by a relatively simple (1 × 5) structure identical to that for Ir(100)(1 × 5) (thereby ignoring the effect of the few different (1 × 5) units containing the dislocation) and therefore an identical calculation is sufficient. We refer to the discussion below about the question of the correspondence of spots between the Ir and Pt structures.

On the other hand, in the rotated-hexagonal-layer model, each of the (1 × 5) units is slightly different from its immediate neighbors. The difference is a small shift (by about (1/14)th of the bond length, i.e. about 0.2 Å) in the registry of the top layer. Since electron multiple scattering is not particularly sensitive to small geometric changes more than a few bond lengths away, because of damping, it should be adequate to assume that the diffraction by any one of these 14 (1 × 5) units is equal to the diffraction by a complete surface with this particular (1 × 5) unit as the repetitive unit cell. Therefore, we may simulate the overall diffraction by the sum of interfering beam amplitudes obtained from a series of relatively simple (1 × 5) structured surfaces, each with a slightly different registry of the top layer. Of course, different registries imply different bucklings perpendicular to the surface, and this is included in the calculation. Because of symmetry and structural-sensitivity considerations, it was found that four different registries would reasonably sample the 14 different registries of the (1 × 5) units. This small number of four comes about because all 14 registries, when mapped in a single (1 × 5) unit cell, correspond to a cumulative shift by only about half a bond length. By symmetry, one half of the registries are identical to the other half, leaving a total relevant shift of about a quarter bond length, i.e. about 0.7 Å. Four equidistant registries are then separated by $0.7/4 \lesssim 0.2$ Å, a lateral shift that does not strongly affect LEED spectra near normal incidence.

To keep the computational effort within acceptable limits, a further slight simplification has to be made. The top layer registry has to satisfy a mirror plane symmetry (the mirror plane being parallel to the 14-fold direction). This restriction induces an error in atomic positions of at most about 0.1 Å and so is thought not to affect the result too much.

Finally, it must be realized that with these simplifications one effectively calculates the intensities of beams in the (1/5)th order positions rather than of the multiplets of beams actually observed (cf. the differences between the Ir(100)(1 × 5) and the Pt(100)($_{-1}^{14} {_5^1}$) patterns). However, it was found experimentally that the different components of these multiplets have very similar *IV* curves, implying that the error in using either of these components or a hypothetical (1/5)th order beam should be small. The error is mainly due to the small difference of at most a few degrees between the emission angles of the multiplet components (this difference is less influential than when the crystal sample is tilted by such angles, since in our present case the incidence direction is not changed at all).

We do not carry out an *R* factor analysis to compare theoretical and experimental LEED *IV* curves for two reasons.

First, the photographic technique produces *IV* curves that in this case have relatively large gaps, since no intensity measurements are made over certain energy ranges of weak intensities. No presently available *R* factor treats such gaps in a fair manner and, in any case, such gaps could induce serious spurious effects in the *R* factor when the inner potential is varied. Second, the experimental curves have not been smoothed, so that any *R* factor using derivatives (i.e. most presently used *R*

Table 1
Surface structure models for which dynamical LEED calculations have been made; explanations are given in the text

Models for Ir(100)(1 × 5), all with 6 phase shifts

			Phase shift	d (Å)
θ = 0°				
1. Hexagonal	Planar	Center/top	AH	1.82 (0.10) 2.72
2. Hexagonal	Planar	Two-bridge	AH	2.20 (0.10) 2.70
3. Hexagonal	1/2 buckling	Two-bridge	AH	2.20 (0.10) 2.70
4. Hexagonal	2/3 buckling	Two-bridge	AH	1.90 (0.10) 2.40
5. Hexagonal	2/3 buckling	Two-bridge	AHF	2.20 (0.10) 2.70
6. Hexagonal	Full buckling	Two-bridge	AHF	1.90 (0.05) 2.15
7. Hexagonal	Full buckling	Two-bridge	AHF	1.90 (0.10) 2.40, uneven contraction
8. Hexagonal	Full buckling	Two-bridge	AH	1.90 (0.10) 2.40, uneven contraction
9. Hexagonal	Full buckling	Center/top	AH	1.82 (0.10) 2.72
10. Hex. missing row	Planar	Center/top	AH	1.82 (0.10) 2.72
11. Hex. missing row	Planar	Two-bridge	AH	2.20 (0.10) 2.70
12. Hex. missing row	Full buckling	Center/top	AH	1.82 (0.10) 2.72
13. Hex. missing row	Full buckling	Two-bridge	AH	2.20 (0.10) 2.70
14. Shifted rows	5-cluster			1.62 (0.10) 2.12
15. Shifted rows	4-cluster		AHF	1.62 (0.10) 2.12

16.	Shifted rows	3-cluster	Perpendicular	AHF	1.62 (0.10) 2.12
17.	CDW	0.1 Å amplitude		AH	1.62 (0.10) 2.12
18.	CDW	0.1 Å amplitude	Angled	AH	1.62 (0.10) 2.12
$\theta = 10°$					
19.	Hexagonal	1/2 buckling	Bridges	AHF	1.90 (0.10) 2.40
$\theta = 20°$					
20.	Hexagonal	1/2 buckling	Bridges	AHF	1.90 (0.10) 2.40

Models for Pt(100)$\left(\begin{smallmatrix}14 & 1 \\ -1 & 5\end{smallmatrix}\right)$ all with $\theta = 0°$

				Phase shift	d (Å)
As one registry of (1 × 5)					
21.	Hexagonal	Full buckling	Two-bridge	5 A	1.85 (0.10) 2.35
22.	Hexagonal	Full buckling	Center/top	5 A	1.85 (0.10) 2.35
23.	Hexagonal	Full buckling	Center/top	6 A	1.85 (0.10) 2.35
24.	Hexagonal	Full buckling	Center/top	6 AF	1.85 (0.10) 2.35
As 14 registries of (1 × 5)					
25.	Hexagonal	Full buckling	Two-bridge	5 A	$D + n \times 0.1$ ($n = -2, -1, ..., 2$)
26.	Hexagonal	Full buckling	Center/top	5 A	$D + n \times 0.1$ ($n = -2, -1, ..., 2$)
27.	Hexagonal	Full buckling	Two-bridge	6 AF	$D + n \times 0.1$ ($n = -2, -1, ..., 2$)
28.	Hexagonal	1/2 buckling	Two-bridge	6 AF	$D + n \times 0.1$ ($n = -3, -2, ..., 1$)

factors) becomes useless. Thus it would be difficult to compare R factor values from this work with those in other work.

3. Results

The surface structures that have been tried with dynamical LEED calculations are listed and detailed in table 1. In this table, the registry of a hexagonal layer ("two-bridge" or "center/top") is designated as in section 5 of paper I. The rotated hexagonal layer for Pt(100) can be "anchored" at the bridge sites or at the center/top sites, and these sites are then chosen to designate the registry of the complete layer. The buckling of a hexagonal layer is described as either "full buckling" or "2/3 buckling" or "1/2 buckling", the non-buckled case being called "planar". Full buckling is obtained by at first assumeding bulk bond lengths between the top and the next layers and then allowing the top layer to *rigidly* shift up and down normal to the surface, so that the buckling is not made dependent on this shift. For 2/3 and 1/2 buckling the fully-buckled top layer is contracted uniformly to 2/3 or 1/2 of its thickness, respectively (thickness being defined as the maximum distance between *nuclear* planes of the buckled layer). The atoms in the planar hexagonal layer are assumed equally contracted parallel to the surface. In the buckled geometries the interatomic distances parallel to the surface are not changed from those in the planar case, although some small (<0.1 Å) differences might occur in reality because of the different perpendicular displacements of the various atoms above the next unreconstructed layer. A test of the effect of relaxing this assumption was made with the somewhat extreme "uneven contraction" model, in which the contraction is confined to one atom in the (1 × 5) unit cell, while the other atoms have diameters equal to their bulk value. Almost no change was observed in the resulting *IV* curves.

The reconstructed top layer has a "*d* spacing" to the next unreconstructed layer. In the (1 × 5) structures this spacing is defined as the smallest of the distances between each nuclear plane of the top layer and the nuclear plane of the square-net second layer. This definition of spacing applies not only to hexagonal layers, but also to the shifted-rows and charge-density-wave (CDW) models. In the $\left(\begin{smallmatrix} 14 & 1 \\ -1 & 5 \end{smallmatrix}\right)$ calculations using a series of different fegistries, the d spacing is referred to the distance D, which is the distance one would obtain by assuming bulk bond lengths between top-and-next-layer atoms. In the shifted-rows models, the shifted atoms are given bulk bond lengths to their neighbors, assuming positions as shown in fig. 9 of paper I, and then the entire 5-atom-per-unit-cell top layer is allowed to *rigidly* shift up and down. In the CDW model the wave-like atomic deviations are either in the direction perpendicular to the surface or "angled". In the latter case, deviations parallel to the surface (in the 5-fold direction) are chosen, but the atoms are allowed to displace at an angle over the underlying atoms, so as to conserve bond lengths, again followed by rigid shifts up and down.

The phase shifts used are described as AH for Arbman–Hoernfelt [4], AHF for the same with correction by Feder [6], A for Andersen [7] and AF for these with correction by Feder [6].

The search procedure through the plausible structures was as follows. The Ir(100)(1 × 5) surface was extensively studied since it has a relatively simple diffraction pattern and less multiple scattering than Pt (cf. section 2), making any results more reliable and more economical to achieve. The largest number of calculations were performed at normal incidence ($\theta = 0°$) to benefit from higher symmetry, using 7 independent beams in the comparison with experiment. Two off-normal angles of incidence ($\theta = 10°$ and $\theta = 20°$) were chosen to further check the hexagonal model, using 13 and 14 independent beams, respectively. This structure was also chosen in the Pt(100)($^{14}_{-1}$ $^{1}_{5}$) analysis, in which various calculations were performed to independently test some of the geometrical variables.

Before the discussion of the comparison between theoretical and experimental *IV* curves, it should be remembered that the quality of agreement between theory and experiment is not expected to be as good as for some other structural determinations. In addition to the usual uncertainties of experiment and theory, the atomic potentials appear to be of somewhat poorer quality, and for Pt(100), various small approximations have had to be introduced (cf. section 2). Also, many more structural parameters could, in principle, be optimized than we have done (e.g. with 6 atoms in the unit cell there are 18 unknown position parameters, not counting possible distortions of the underlying atoms of the substrate).

3.1. The reconstructed Ir(100) surface

A selection of calculated *IV* curves for Ir(100)(1 × 5) are compared with experiment in figs. 1–4. This selection exhibits the level of agreement between experiment and calculation and various trends with varying parameters. Lack of space prohibits the inclusion of enough figures to provide a basis for selection of the optimum geometry.

The level of agreement seen in figs. 1–4 is inferior to that usually encountered for "correct" structures. But, apart from the inherent complexity of this sytem, it must also be kept in mind that we have analyzed 139 structures for Ir(100) (1 × 5) and that the agreement obtained for the few best structures is markedly superior to that for all other structures. The implication is that we have, in the language of *R* factors, at least approached local minima, rather than hit-or-miss agreement.

In examining all calculated *IV* curves, it emerges that for the hexagonal model of Ir(100)(1 × 5) the theory and experiment clearly agree best if the two-bridge registry rather than the center/top registry is assumed (cf. fig. 9 of paper I). Furthermore, a 1/2 or 2/3 buckling appears best, with a *d* spacing of 2.2 ± 0.1 Å. So the bridge-positioned surface atoms have essentially the bulk bond length to the next-layer atoms and the reduced buckling implies that those atoms sticking out
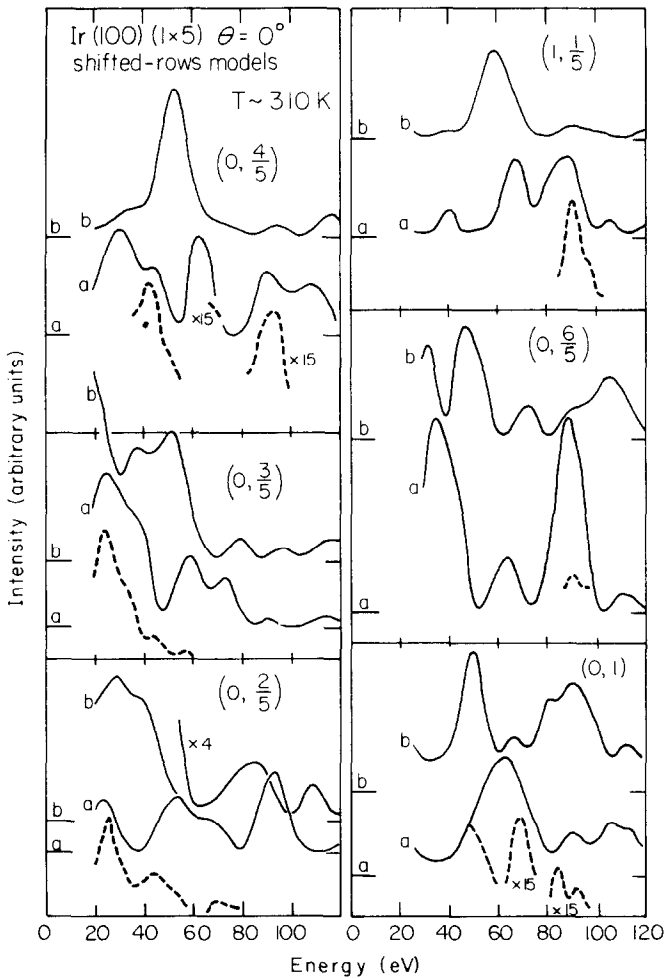
Fig. 1. Experimental (dashed lines) and theoretical (continuous lines) *IV* curves for Ir(100) (1 × 5) with shifted-rows geometries. Curves labelled (a) 5-atom clusters with *d* spacing of 1.62 A. Curves labelled (b) 3-atom clusters with *d* spacing 2.12 A.

above the bridged ones are drawn in somewhat toward the bulk, smoothing the surface. As a consequence, the most protruding atoms have bond length contractions of 6 or 9%, depending on whether one chooses 2/3 or 1/2 buckling. The average contraction of the backbond lengths are then 3 or 4%, respectively, with an uncertainty of ±3% due to the uncertainty of ±0.1 Å in determining the *d* spacing (the backbonds are the bonds between atoms in the first and second layers). Thus our best estimate is: bond length contractions for the various inequivalent surface atoms from 0 ± 3% to 7.5 ± 3% averaging at 3.5 ± 3%.
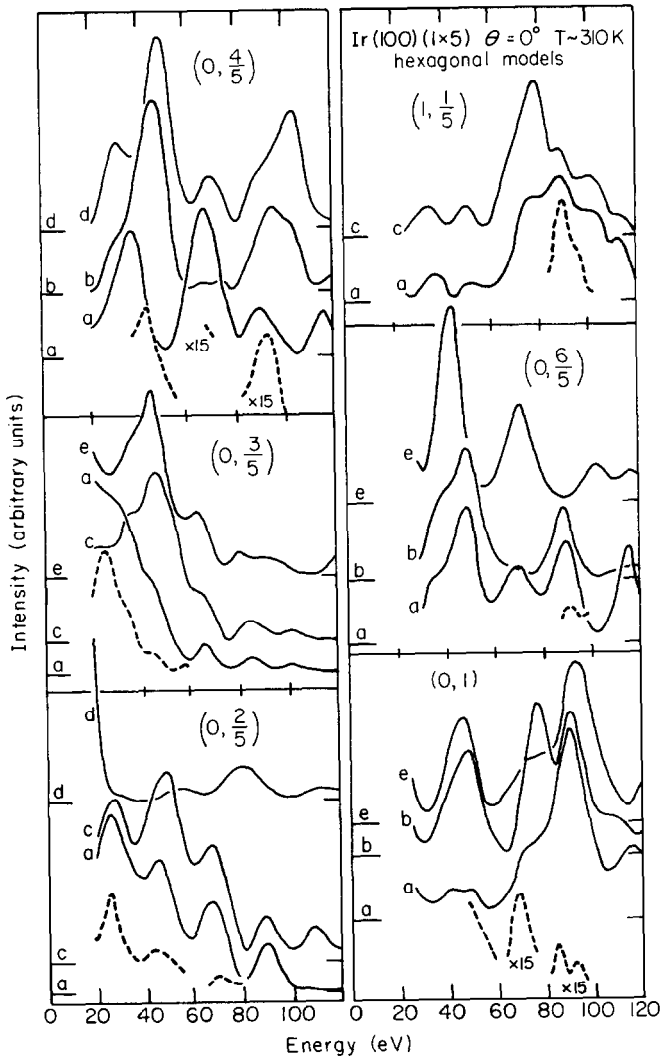
Fig. 2. As fig. 1, but comparing various hexagonal models, all with a d spacing of 2.2 A: (a) two-bridge registry, 1/2 buckling, Feder phase shifts; (b) as (a) without Feder correction; (c) two-bridge registry, full buckling, no Feder correction; (d) two-bridge registry, no buckling (planar), no Feder correction; (e) center/top registry, full buckling, no Feder correction.

The off-normal incidence calculations for the hexagonal model (see table 1) are found to slightly favor a d spacing of 2.0–2.1 Å over other values. However, the agreement between theory and experiment is of a lower quality than at normal incidence. The calculated intensity curves suffer because of some isolated instabili-
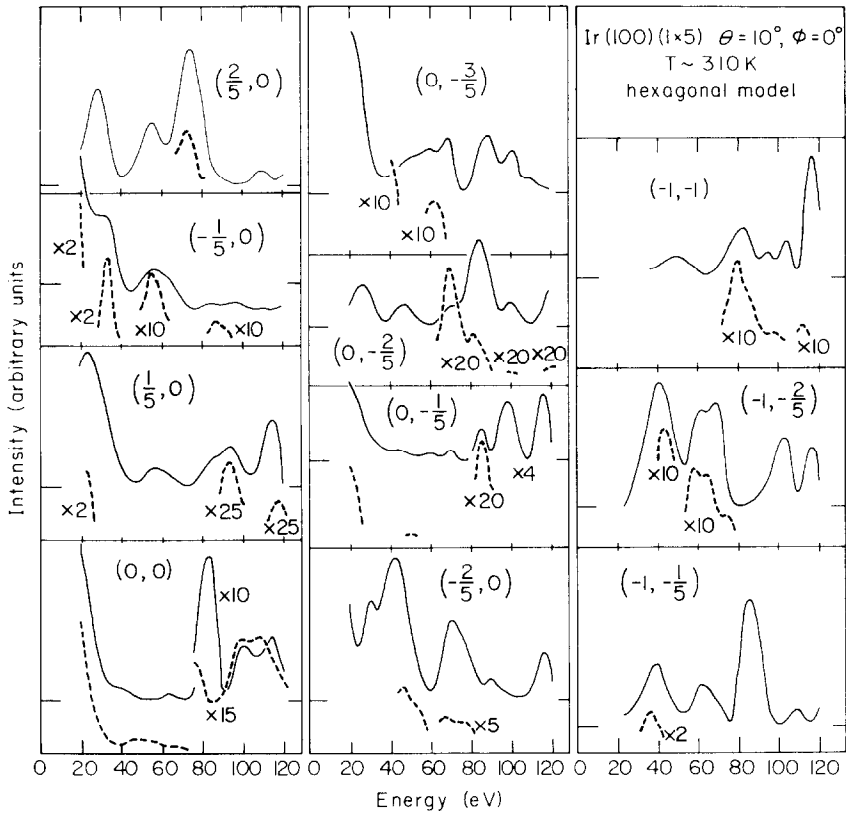
Fig. 3. As fig. 1, but for off-normal incidence ($\theta = 10°$, $\phi = 0°$). The d spacing is 2.1 Å, with two-bridge registry, 1/2 buckling and Feder phase shifts.

ties in the RSP convergence at energies above about 90 eV at off-normal incidence. Therefore, we shall give the normal-incidence results a greater weight and interpret the off-normal incidence results as not contradicting the normal-incidence results.

Among the shifted-rows models (cf. fig. 11 of paper I) the 5-cluster structure with $d = 1.62 \pm 0.1$ Å gives the best agreement with experiment followed by the 3-cluster structure with $d = 2.12 \pm 0.1$ Å. In each of these cases the d spacing represents the distance of top-layer atoms in hollow sites (3 of the 5 atoms in the unit cell are in hollow sites), and thus the spacings of 1.62 ± 0.1 and 2.12 ± 0.1 Å are to be compared with the bulk value to 1.92 Å for this spacing. These two results therefore correspond to changes of $-15 \pm 5\%$ and $+10 \pm 5\%$, respectively, in the d spacings for those hollow-site atoms with respect to an ideal termination of the bulk, and these values translate to changes of $-5 \pm 1.5\%$ and $+3 \pm 1.5\%$, respectively, in the bond lengths with respect to the bulk value. Some additional shifts
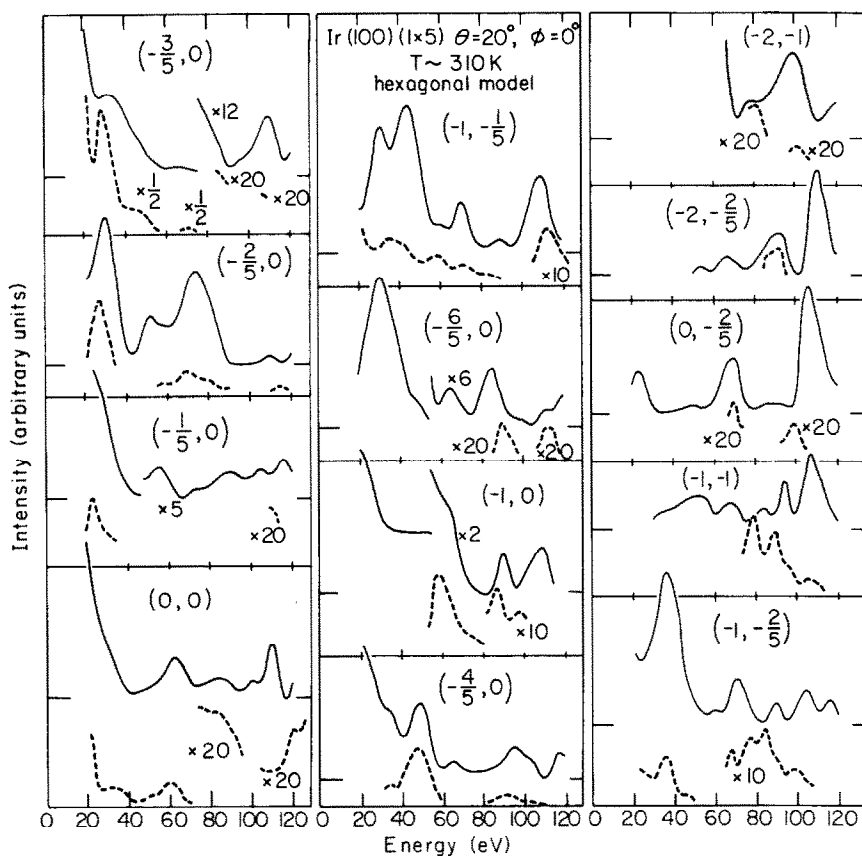
Fig. 4. As fig. 3 for $\theta = 20°$, $\phi = 0°$.

of the already shifted rows of atoms or of the unshifted top-layer atoms might slightly alter these results. We have not attempted to further optimize the shifted-rows model, because very many minor modifications would have to be tried out, with little qualitative improvement to be expected.

The remaining structures listed in table 1 for Ir(100)(1 × 5) can be rejected immediately on the basis of the lack of any correspondence between the theoretical and experimental *IV* curves at normal incidence. These are the planar hexagonal models with either of the two indicated registries, the hexagonal models with missing rows, whether planar or buckled, with either registry, and the CDW models. In the latter case the weakness of all calculated extra beams (one to two orders of magnitude less than the integral order beams) already eliminated the CDW models. In addition the detailed features of the *IV* curves do not match, as is the case for the other structures.

Comparing the results for the shifted-rows models and those for the hexagonal layer for Ir(100)(1 × 5), it appears difficult to make a choice on the basis of the IV curves alone. Although the agreement between theory and experiment is slightly
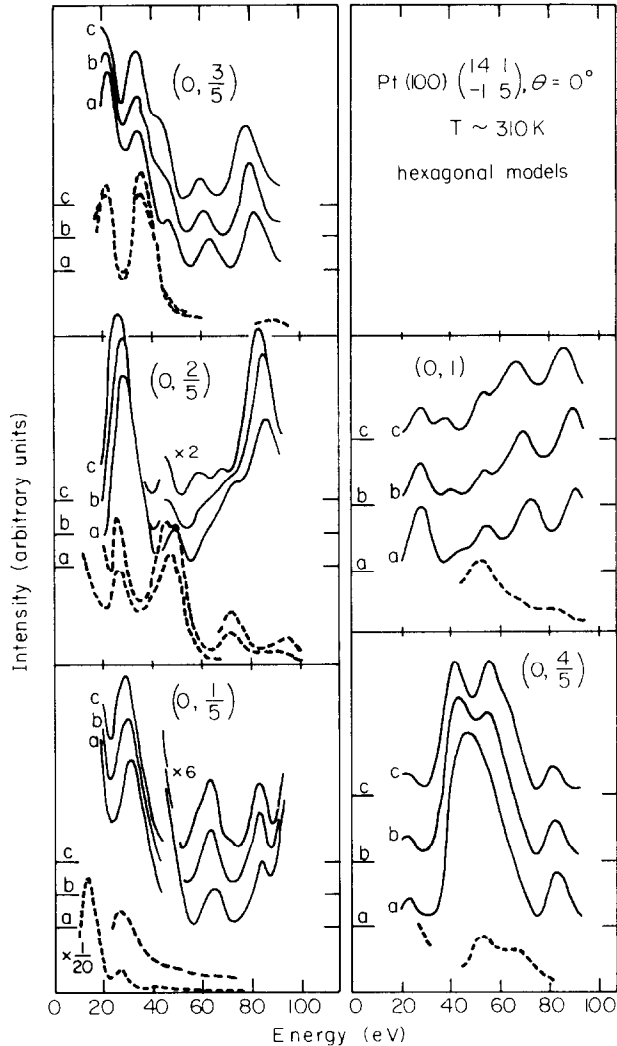

Fig. 5. Experimental (dashed lines) and theoretical (continuous lines) IV curves for Pt(100) ($_{-1}^{14}$ $_{5}^{1}$) with a 1/2 buckled hexagonal top layer in two-bridge registry, using Feder phase shifts. The d spacing is $d = D - 0.3$ Å (curves (a)), $d = D - 0.2$ Å (curves (b)), and $d = D - 0.1$ Å (curves (c)), where D is defined in the text. Where pairs of dashed lines occur, they correspond to different components of split spots (fig. 3 of paper I).

better for the hexagonal model, it must be recognized that more optimization of parameters was performed with this model, so that a choice is not warranted at this point.

3.2. The reconstructed Pt(100) surface

For Pt(100)($_{-1}^{14}$ $_5^1$), a selection of calculated *IV* curves is shown in fig. 5. We found that the hexagonal model fits best with experiment for 1/2 buckling and the two-bridge registry. A contraction by 0.1 to 0.3 Å perpendicular to the surface seems favored, depending on the choice of muffin-tin constant. This contraction represents a 4.2 to 12.6% reduction in the *d* spacing of the top-layer atoms, i.e. on the average about 6.3% backbond length reduction. The uncertainty in this result is hard to estimate, considering the complexity of the model. The shifted-rows models were not tried for Pt.

4. Discussion

We first summarize the results presented in the preceding section. For Ir(100) (1 × 5) the hexagonal model with two-bridge registry (cf. fig. 9 of paper I, left) and 2/3 or 1/2 buckling and a *d* spacing of 2.2 ± 0.1 Å is the favored structure. A shifted-rows model in 5-cluster arrangement, cf. fig. 11c of paper I, with *d* spacing of 1.62 Å is also acceptable (a further 3-cluster model, cf. fig. 11e of paper I, with *d* spacing of 2.12 Å is somewhat less likely on the basis of the *IV* curves). For Pt(100)($_1^5$ $_{14}^1$) the hexagonal model described above with a rotation of about 0.7° gives reasonable agreement with experiment, cf. fig. 6 of paper I.

We are left with two basic possible models. The hexagonal model is simple to imagine, but involves conceptual difficulties in terms of excess concentration of atoms and, in the case of platinum, an additional rotation. The shifted-rows model solves those particular difficulties, but introduces new ones related to more complicated bond length changes and domain arrangements.

4.1. Other reconstructions

At this point it is of interest to mention other metal surface reconstructions. On the cooled clean W(100) crystal face a c(2 × 2) pattern is observed. The *IV* curves from this surface structure have been analyzed [10], showing that zigzag chains of W surface atoms probably form by slight displacements from the ideal positions. This structure can be understood in terms of a charge density wave [11]. The cooled clean Mo(100) surface exhibits a split c(2 × 2) pattern [12] that may have structure similar to W(100)c(2 × 2) and then also can be interpreted as being due to a charge density wave.

The clean Ir(110) and Au(110) surfaces have (1 × 2) structures. These have been

suggested [5,13] to probably consist of alternately missing rows, producing a microfacetted structure, each microfacet having the close-packed atomic arrangement of a (111) face. This result is an argument in favor of a hexagonally close-packed top layer for Ir, Pt and Au(100). Furthermore, relatively large backbond length contractions of about 3% occur in this case. Pt(110) also can exhibit (1 X 2) structures, but several attempts at determining these structures have not yet led to conclusive results.

Finally, clean Au(111) has a reconstruction [14] that may consist of a 4.55% uniaxially contracted top hexagonal layer (although a charge-density-wave structure is also possible), as discussed in section 4 of paper I.

4.2. Bond lengths

Whether one favors the hexagonal or the shifted-rows model, it appears that bond length changes are an important aspect of the reconstructions. In the hexagonal models of reconstruction, we find that bond lengths in the Ir, Pt and Au exhibit contractions within the hexagonal layer of 1%, 3% and 4.2%, respectively (these numbers are averages over different directions parallel to the surface and take the buckling into account). Backbonds are reduced by, on the average, 3.5% and 6.3%, respectively for Ir and Pt. For the shifted-rows model, the best structure for Ir gives a bond length contraction between non-shifted top-layer and next-layer atoms of 5% (the overall average bond length change cannot be reliably obtained without additional LEED calculations to optimize the structure). Such values are compatible with bond length contractions observed at other, mostly unreconstructed, metal surfaces [1], which range from 0 to 4%. However, so far contractions were only clearly observed on the less-densely-packed surfaces, such as fcc(110), fcc(311), bcc(100) and bcc(111). Diatomic molecules show rather larger contractions, such as 14% for Au_2 and 13% for Cu_2 as compared with bulk Au and Cu bond lengths, respectively [15].

Bond length contractions have also been observed in small clusters of metal atoms. Platinum clusters of diameters 12 and 20 Å (containing about 60 and 280 atoms, respectively) have average Pt—Pt bond length reductions of 7% and 5%, respectively [16]. Slightly larger clusters have less contraction: 0.5% for 38 Å-diameter Pt clusters [17], 0.3% for 35 Å-diameter Au clusters [18], 0.6% for 40 Å-diameter Ag clusters [19] and 0 ± 0.1% for clusters of Cu with diameters of 38 Å and more [17]. Note that platinum and gold clusters contract significantly, but not the copper clusters. This fits the pattern of surface reconstructions on Pt and Au surfaces and their absence on Cu surfaces. However, silver appears to behave more like platinum and gold in clusters, unlike the behavior at surfaces, where silver does not reconstruct. As is well known [20], bond lengths increase monotonically with the number of nearest neighbors, i.e. the coordination number, and thus a contraction is indeed expected for surface atoms (this would also favor a reduction in any buckling of the hexagonal layer, in agreement with our observations). In fig. 6 we show
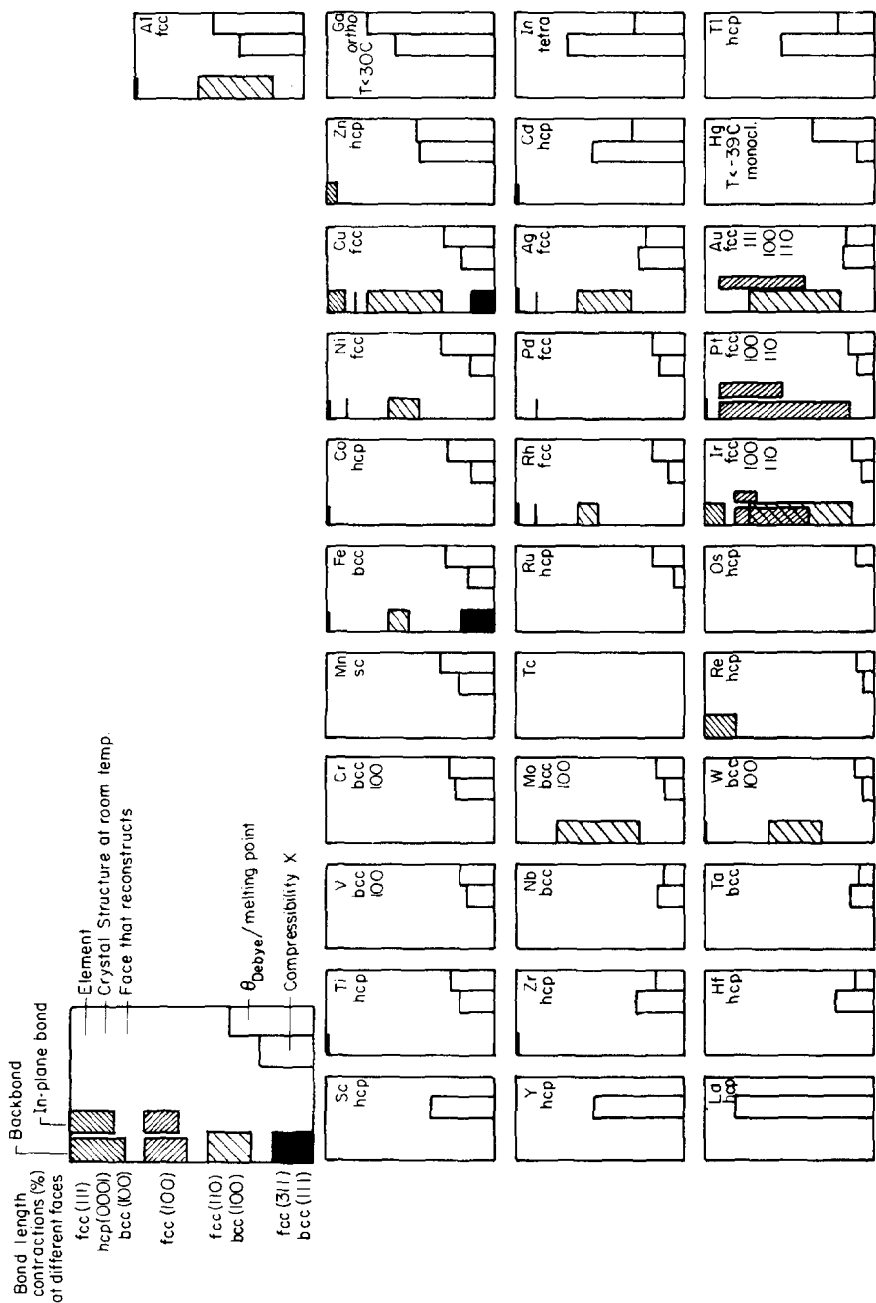
Fig. 6. Part of the Periodic Table showing occurrences of clean-surface reconstructions, indicated by the Miller indices of the affected faces. For each element, bars at left have heights proportional to surface bond length contractions for different surface orientations, while other bars are proportional to selected bulk material constants (see key at top). A distinction is made between backbonds (between topmost and next atomic layers) and in-plane bonds parallel to the surface. The heights of the drawn bars can be compared directly from element to element. The plotted data, covering only the known results, are based mainly on refs. [31–33].

the bond length contractions observed at surfaces [1] assuming for simplicity 0% for many fcc(100), fcc(111) and bcc(110) surfaces, since most results for these surfaces give the bulk value within the uncertainty of the LEED method. We shall discuss these in more detail below.

It is interesting to add observations made during epitaxy of overlayers of one metal on substrates of another. A simple monolayer of Au or Ag deposited on Cu(100) produces different superstructures [15], despite virtually identical bulk Au and Ag bond lengths. These structures can both be interpreted as hexagonal overlayers, but then the Au layer requires a 3.3% larger uniaxial contraction than does the Ag layer. Thus Au has a greater tendency to bond length reduction than Ag. In another comparison, we start with the fact that the bulk Au lattice constant is about 4.3% larger than that of Pt. A Au monolayer deposited on Pt(100) produces a square lattice with the Pt lattice constant [21], indicating a 4.3% contraction of the Au—Au distance.

Note, among the above results, the formation of contracted square-lattice overlayers, also observed for Au on Pd(100) [15]. It appears that hexagonal layers are not the universal form of reconstruction even in the case of misfits, but we cannot assess whether these square-lattice overlayers are possibly only metastable phases that could transform to more stable hexagonal (or other) overlayers. Note also the dependence of the overlayer contractions on the substrate lattice constant. There is an interplay between the substrate lattice and the overlayer that, for a given adsorbate species, produces overlayer lattices different both in symmetry (square versus hexagonal, etc.) and in size, depending on the particular substrate [22].

Clearly then the Ir, Pt and Au(100) reconstructions involve bond length contractions. This may be the very reason for the reconstructions: in the unreconstructed surface, the bonds parallel to the surface may be stretched too much as a consequence of the atomic contraction, which therefore could make a reconstruction energetically favorable in which shorter bond lengths predominate. Frank and Van der Merwe [23] have proposed a theory of this competition between pseudomorphism (crystal growth with the substrate's lattice) and independent lattice growth. This theory predicts that for typical metals up to a 9% difference in lattice constants can be accommodated by strain for one monolayer deposited on a substrate and that only a smaller difference can be accommodated for multilayers. This behavior is observed for some of the above-mentioned cases, such as for the pseudomorphism of a monolayer of Au on Pd(100) or on Pt(100), but apparently not for other cases, such as for the 5% smaller monolayer of Pt on Au(100) or for the clean reconstructed Pt(100) and Au(100) structures, although the actual surface lattice constants in these examples differ by less than 9%.

4.3. Mechanism of reconstruction

Bond length contractions are not necessarily the only mechanism for reconstruction that is operative for the (100) crystal faces of Ir, Pt, and Au (as noted in ref.

[15]). It appears that other effects such as rehybridization of bonding orbitals may play an important role as well. In this respect, Palmberg and Rhodin [15] already pointed out the unusual electronic characteristics of Pt and Au (and predicted, before its observation, that Ir might have a similar reconstruction [24]). For Pt and Au, there is a relatively small activation energy between the atomic ground state and a state in which a 5d electron is promoted to a 6s or 6p orbital. Thus a reconstruction may induce a sufficient gain in energy to offset that small promotion energy. Such a mechanism is often invoked to explain bulk phase transformations [25] and may very well operate in the present case as well. But it must be pointed out that the electronic properties of Cu are not very different from those of Au in this respect, and Cu(100) is not known to reconstruct. Furthermore, an investigation of known differences in cohesive energies for different bulk phases of various elements [26], either experimentally measured or theoretically calculated for non-existing phases, shows that from the point of view of phase transformations Pt and especially Au are in fact unlikely to reconstruct. Au has one of the largest differences in cohesive energies of all metals between bulk phases. Furthermore, V, Cr, Mo and W, all of which exhibit surface reconstructions, also have relatively large differences in cohesive energies between different bulk phases.

4.4. Correlations with material constants

One may explore the possibility that the observed bond length contractions at Ir, Pt and Au surfaces, as well as the tendency of these surfaces to reconstruct, correlate with any other physical properties of these metals. Obvious quantities to consider are those describing the stiffness of the lattice such as the Debye temperature, the melting point, the cohesion energy and elastic constants. First, a clear trend is found in the bond length contractions themselves (see fig. 6). The bond length contractions tend to increase markedly (only identical crystallographic surface orientations must be compared), as one goes to the right in the Periodic Table among the fcc metals, for which the most data are available. These bond length contractions also correlate well with the mechanical softness of the elements. Fig. 6 includes the compressibility χ as an example; χ also increases towards the right in the Periodic Table among the fcc metals. On the other hand, although the 5d metals exhibit larger bond length contractions than 4d or 3d metals, their compressibility is not smaller; W and Ir are well known to be hard materials. In fact, it is interesting to note that throughout the Periodic Table (fig. 6) the compressibility tends to be locally minimized near metals that reconstruct.

Among various other materials constants and combinations thereof, we have only found a clear-cut trend for the ratio of bulk Debye temperature to melting point. This ratio is unusually small for those metals that reconstruct. Since, on the one hand, a low Debye temperature is related to weak restoring forces of the vibrating atomic cores (where the mass is concentrated), while, on the other hand, a high melting point is related to strong chemical bonds, this unusual combination

may be pictured as a relatively free vibration of the atomic cores within a set of bonding orbitals that are more rigidly held in place by the neighboring atoms. In more conventional terms, this would correspond to a relatively high polarizability of the 5d metal atoms, coupled with strong bonding. A related point of view is that of the soft-phonon theory of reconstructions [27]. Abnormally low phonon frequencies (which we tentatively relate here to lower Debye temperatures) are taken as a sign of propensity to reconstruction.

4.5. Prospects for finding other metal surface reconstructions

Finally, let us consider which other metals besides those mentioned here might exhibit clean-surface reconstructions. Since many 5d metals have small ratios of Debye temperature to melting point, one might expect, for example, rhenium and osmium to reconstruct, even though their bulk has the hcp structure. Since several bcc(100) surfaces reconstruct it would be useful to investigate, for example, Nb(100) and Fe(100) at low temperature (they do not reconstruct at room temperature) [28,29]. Metals which have bulk phase transitions might reconstruct at their surfaces. Mn, Co and Tc are good candidates (but the surfaces of Co(111) and Co(0001) are known to have their respective bulk structure [30] at room temperature and above). One may also expect non-close-packed surfaces to reconstruct more easily than close-packed surfaces, since W(110), Ir(111) and Pt(111) apparently do not reconstruct, while W(100), Ir(100), Ir(110), Pt(100) and Pt(110) do.

5. Conclusions

The structural analysis of the clean reconstructed Ir, Pt and Au(100) surfaces suggests that a close-packed hexagonal top monolayer can explain each of the observed reconstructions. However, a second model, based on pairs of shifted atomic rows, is also compatible with the observed LEED patterns and intensities, although it is in disagreement with other results, mainly from ion scattering experiments.

For Ir and Pt, the preferred model for the hexagonal top layer has the "two-bridge" registry, 1/2 to 2/3 of full buckling and average contractions of backbonds (i.e. bonds between atoms in the first and second layers) of $3.5 \pm 3\%$ and 6.3%, respectively (cf. fig. 9 of paper I). Bond length contractions parallel to the surface are on the average about 1% for Ir, 3% for Pt and 4.2% for Au (cf. fig. 6 of paper I). The hexagonal layer has close-packed rows of atoms aligned with a [110] direction for Ir and Au, but rotated by about 0.7° for Pt. (The figures for Pt apply to the $\begin{pmatrix} 14 & 1 \\ -1 & 5 \end{pmatrix}$ structure; slightly different values would apply for the closely-related $\begin{pmatrix} 14 & 1 \\ 0 & 5 \end{pmatrix}$, $\begin{pmatrix} 14 & 1 \\ -3 & 10 \end{pmatrix}$ and other structures.)

The shifted-rows model, examined for the reconstructed Ir(100) surface only, fits best to experiment with 5-atom clusters (cf. fig. 11c of paper I) with backbond length contractions for the unshifted atoms of about $5 \pm 1.5\%$.

We can rule out several classes of reconstruction for Ir, Pt and Au(100) surfaces: non-buckled hexagonal top layers, some missing-row models, several shifted-rows models and charge-density-wave models. Also no abrupt dislocations other than at domain boundaries may occur for Pt and Au(100).

Thus the most likely reconstructions of Ir, Pt and Au(100) involve the formation of contracted and sometimes rotated hexagonal monolayers with a surface density of atoms increased by 20%, 23.7% and 27.7%, respectively, relative to a bulk (100) layer. The reason for this reconstruction might be a reduced bond length between surface atoms, which induces too much strain in the unreconstructed geometry. It may also be due to a decreased surface energy as a result of the closer packing.

We find a correlation of the occurrence of surface reconstructions in several 5d metals with a relatively small bulk compressibility and with a relatively small ratio of Debye temperature to melting point for the 5d metals. Thus a connection with the soft-phonon theory of reconstruction may exist. It also follows that other 5d metals, such as Ta, Re and Os, may exhibit surface reconstructions. In addition, non-close-packed suraces seem more likely to reconstruct than close-packed surfaces. Also, bcc(100) surfaces may reconstruct in general at low temperatures, as well as metals with bulk phase transitions.

It is not clear that experiments with existing surface analytical techniques other than LEED will be able to more closely determine the reconstruction geometries of Ir, Pt and Au(100). But in the near future, Low-Energy Ion Scattering Spectroscopy and Atomic Diffraction may be able to quantitatively determine the roughness (buckling) of the topmost atomic layer and thereby further differentiate between the hexagonal and the shifted-rows models. Also, Atomic Resolution Electron Microscopy may soon be able to provide further information about the relative atomic locations at surfaces.

Concerning possible future refinements in the LEED analysis, it must be recognized that surfaces with large unit cells present many a priori possible structures and that therefore the inherent limitations of this technique cannot guarantee that only one structure will prove suitable: in general, several structures may appear acceptable. To reduce the number of acceptable structures and minimize error bars on atomic locations requires a simultaneous improvement in many theoretical and experimental details. As a specific point, we mention the need for better electron–atom scattering potentials for the 5d metals.

References

[1] M.A. Van Hove and S.Y. Tong, Surface Crystallography by LEED (Springer, Heidelberg, 1979).

[2] J.B. Pendry, Low Energy Electron Diffraction (Academic Press, London, 1974).

[3] C.-M. Chan, S.L. Cunningham, M.A. Van Hove, W.H. Weinberg and S.P. Withrow, Surface Sci. 66 (1977) 394.

[4] G.O. Arbman and S. Hoernfelt, J. Phys. F2 (1972) 1033.

[5] C.-M. Chan, M.A. Van Hove, W.H. Weinberg and E.D. Williams, Solid State Commun. 30 (1979) 47; Surface Sci. 91 (1980) 440.

[6] R. Feder, private communication.

[7] O.K. Anderson, Phys. Rev. B2 (1970) 883.

[8] (a) L.L. Kesmodel and G.A. Somorjai, Phys. Rev. B11 (1975) 630; Surface Sci. 64 (1977) 342.
(b) D.L. Adams, H.B. Nielsen and M.A. Van Hove, Phys. Rev. B20 (1979) 4789.

[9] R. Feder, Surface Sci. 68 (1977) 229.

[10] R.A. Barker, P.J. Estrup, F. Jona and P.M. Marcus, Solid State Commun. 25 (1978) 375.

[11] (a) J.E. Inglesfield, J. Phys. C11 (1978) L69.
(b) E. Tosatti, Solid State Commun. 25 (1978) 637.

[12] T.E. Felter, R.A. Barker and P.J. Estrup, Phys. Rev. Letters 38 (1977) 1138.

[13] W. Moritz and D. Wolf, Surface Sci. 88 (1979) L29.

[14] J. Perdereau, J.P. Biberian and G.E. Rhead, J. Phys. F4 (1974) 798.

[15] P.W. Palmberg and T.N. Rhodin, J. Chem. Phys. 49 (1972) 134.

[16] B. Moraweck, C. Clugnet and A.J. Renouprez, Surface Sci. 81 (1979) L631; and A.J. Renouprez, communication at Surfaces Meeting, Cocoyoc, Mexico, 1980.

[17] H.J. Wasserman and J.S. Vermaak, Surface Sci. 32 (1972) 168.

[18] C.W. Mays, J.S. Vermaak and D. Kuhlmann-Wilsdorf, Surface Sci. 12 (1968) 134.

[19] H.J. Wasserman and J.S. Vermaak, Surface Sci. 22 (1970) 164.

[20] L. Pauling, The Nature of the Chemical Bond (Cornell Univ. Press, 1973).

[21] J.W.A. Sachtler, private communication.

[22] A more complete review of the structure of metal monolayers on metal substrates is found in ref. [45b] of paper I, and in: J.P. Biberian and G.A. Somorjai, to be published.

[23] F.C. Frank and J.H. van der Merwe, Proc. Roy. Soc. (London) A189 (1949) 205.

[24] T.N. Rhodin, P.W. Palmberg and E.W. Plummer, in: Structure and Chemistry of Solid Surfaces, Ed. G.A. Somorjai (Wiley, New York, 1969).

[25] L. Brewer, Science 161 (1968) 115; and in: Phase Stability in Metals and Alloys, Eds. P. Rudman, J. Stringer and R.I. Jaffee (McGraw-Hill, New York, 1967) p. 39.

[26] L. Brewer, The Cohesive Energies of the Elements (Lawrence Berkeley Laboratory Report 3720, 1975).

[27] See, for example, S.E. Trullinger, S.L. Cunningham and D.L. Mills, Solid State Commun. 13 (1973) 975.

[28] D. Tabor and J.M. Wilson, Surface Sci. 20 (1970) 203.

[29] K.O. Legg, F. Jona, D.W. Jepsen and P.M. Marcus, J. Phys. C10 (1977) 937.

[30] B.W. Lee, R. Alsenz, A. Ignatiev and M.A. Van Hove, Phys. Rev. B17 (1978) 1510.

[31] G.A. Somorjai and M.A. Van Hove, in Structure and Bonding, Vol. 38 (Springer, Heidelberg, 1979) p. 1.

[32] G.V. Samsonov, Ed., Handbook of the Physiochemical Properties of the Elements (IFI/Plenum, New York, 1968) pp. 397–398.

[33] International Tables for X-ray Crystallography, Vol. III (Kynoch, Birmingham, 1962) pp. 233–241.